

# No More Sliding Window: Efficient 3D Medical Image Segmentation with Differentiable Top- $k$ Patch Sampling

Young Seok Jeon, Hongfei Yang, Huazhu Fu, and Mengling Feng

**Abstract**—3D models are favored over 2D for 3D medical image segmentation tasks due to their ability to leverage inter-slice relationship, yielding higher segmentation accuracy. However, 3D models demand significantly more GPU memory with increased model size and intermediate tensors. A common solution is to use patch-based training and make whole-volume predictions with sliding window (SW) inference. SW inference reduces memory usage but is slower due to equal resource allocation across patches and less accurate as it overlooks global features beyond patches.

We propose NMSW-Net (No-More-Sliding-Window-Net), a novel framework that enhances efficiency and accuracy of any given 3D segmentation model by eliminating SW inference and incorporating global predictions when necessary. NMSW-Net incorporates a differentiable Top- $k$  module to sample only the relevant patches that enhance segmentation accuracy, thereby minimizing redundant computations. Additionally, it learns to leverage coarse global predictions when patch prediction alone is insufficient. NMSW-Net is model-agnostic, making it compatible with any 3D segmentation model that previously relied on SW inference.

Evaluated across 3 tasks with 3 segmentation backbones, NMSW-Net achieves competitive or sometimes superior accuracy compared to SW, while reducing computational complexity by 90% (87.5  $\rightarrow$  7.95 TFLOPS), delivering 4 $\times$  faster inference on the H100 GPU (19.0  $\rightarrow$  4.3 sec), and 7 $\times$  faster inference on the Intel Xeon Gold CPU (1710  $\rightarrow$  230 seconds).

**Index Terms**—Deep Learning, 3D Medical Image Segmentation, Differentiable Top- $k$  Sampling, Gumbel-Softmax Trick, Efficient Inference, Sliding Window Inference.

## I. INTRODUCTION

### A. 2D vs 3D model for 3D Medical Image Segmentation

2D and 3D segmentation models possess distinct advantages and disadvantages when applied to 3D medical image seg-

This paragraph of the first footnote will contain the date on which you submitted your paper for review. It will also contain support information, including sponsor and financial support acknowledgment. For example, "This work was supported in part by the U.S. Department of Commerce under Grant BS123456."

Y.S. Jeon is with the Institute of Data Science, National University of Singapore, Singapore (e-mail: youngseokjeon74@gmail.com).

H. Yang is with the Saw Swee Hock School of Public Health, National University of Singapore, Singapore (e-mail: hfyang@nus.edu.sg).

H. Foo is with the Agency for Science, Technology and Research (A\*STAR), Singapore (e-mail: hzfu@ieee.org).

M. Feng (coresponding) is with the Saw Swee Hock School of Public Health, National University of Singapore, Singapore (e-mail: ephfm@nus.edu.sg).

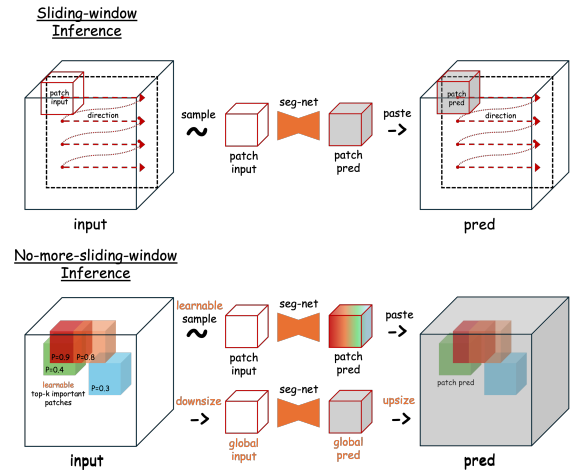


Fig. 1. NMSW-Net offers an efficient alternative to the computationally intensive Sliding Window inference method, which allocates equal resources across all patches. In contrast, NMSW-Net incorporates a differentiable patch sampling module to select a handful of patches that enhance segmentation accuracy. Additionally, NMSW-Net learns to incorporate coarse global prediction for the objects that require broader feature context.

mentation tasks. For 2D models, the 3D input is destructured into a batch of 2D slices, typically along the axial direction, with predictions made independently for each slice. While 2D models are computationally efficient, they fail to capture inter-slice relationships, potentially reducing the accuracy of the final whole-volume prediction.

3D models, in contrast, take the whole 3D input without the destructuring. The model weights extend along the axial direction to capture inter-slice relationships, resulting in improved accuracy [1], [2]. However, this approach comes at the cost of increased computational demands.

### B. Computational Inefficiency of 3D models

Increased computational demand and memory requirements present a significant bottleneck for all 3D segmentation models, regardless of their underlying backbone structure—whether Conv-net [3], Self-attention [4], or State-Space models [5]. Using ConvNet as an example, increasing the convolutional kernel dimension from  $k \times k$  to  $k \times k \times k$  amplifies the number of multiplications and additions required to produce each output pixel/voxel by a factor of  $k$ .

More critically, the memory required to store intermediate tensor outputs during backpropagation also increases, as it now includes an additional depth dimension. This challenge becomes particularly pronounced when using parallelizable matrix multiplication-based convolution algorithms, such as im2col [6] or Winograd convolutions [7].

Transformer models are no exception to the challenges of increased memory usage and computational costs. While their architecture remains largely consistent when transitioning from 2D to 3D, the addition of tokens in the axial dimension increases the size of the self-attention matrix quadratically. For example, if a token is worth a patch of size  $16 \times 16 \times 16$ , a CT scan of size  $512 \times 512 \times 512$  yields 32,768 tokens ( $32 \times 32 \times 32$ ), resulting in a self-attention matrix of size  $32,768 \times 32,768$ .

### C. Reducing 3D Model's Memory with Sliding Window

Patch-based training, coupled with Sliding-Window (SW) inference, is the predominant method to address the substantial memory requirements of 3D models. Rather than processing the entire volume in a single step, patch-based training randomly samples a set of patches that are significantly smaller than the actual volume. To generate the final whole-volume prediction using the patch-trained model, SW, as shown in Figure 1, is employed. SW makes sequential predictions on patches sampled at uniform intervals with some overlap (typically between 25-50% [9]). The overlapping predictions are then aggregated into the final whole-volume prediction with an appropriate post-processing step.

### D. Inefficiency and prediction bias in SW-inference

Although SW is memory-efficient due to its constrained input patch size, it has significant drawbacks, including slower inference speed and increased computational demands. Because the patch-based model is not trained to rank patch importance, SW adopts a conservative approach, segmenting all patches with equal computational resources, even those that clearly do not contain objects of interest or the object is simple enough for a less complex model to handle equally well.

A typical ensemble UNet model [9] takes nearly a minute to perform a full SW on a whole-volume size of  $512 \times 512 \times 458$  using an NVIDIA GeForce RTX 3090 GPU [10]. Moreover, health practitioners often rely on on-device processors for model inference, where the speed drops significantly, taking over 10 minutes (Table I).

SW is not only slow during inference, but could potentially lead to poorer performance due to small patch size. One unique aspect of medical image segmentation, compared to generic segmentation tasks on natural images, is the need for global features, such as location, which greatly help in distinguishing objects that may appear similar at a local level. Patch-trained models, however, may miss these global aspects. The most common approach to address this inherent limitation in patch-based models is to train another model that segments using a low-resolution input [9]. However, this adds additional complexity to a model that is already computationally expensive.

### E. How do Radiologists Segment

How do radiologists segment objects in 3D medical images? Investigating their segmentation protocols could provide insights for creating a more computationally efficient inference method. Unlike the SW inference, radiologists follow a distinct, streamlined approach. Their process typically involves three steps:

- 1) **Initial Assessment:** Radiologists begin by quickly skimming through the slices to grasp the anatomical context and locate the regions of interest (ROIs). During this step, they also assess and rank the segmentation difficulty of each ROI.
- 2) **Preliminary Segmentation:** Next, they begin segmenting ROIs identified as lower in difficulty in a semi-automated manner using machine learning or traditional labeling tools.
- 3) **Focused Refinement:** In the final step, radiologists allocate additional time to refine the coarse segmentation output from the previous step, based on the rankings established in the initial assessment.

This workflow enables radiologists to min-max efficiency and accuracy.

### F. No-More-Sliding-Window Inference

We introduce a novel and computationally efficient inference framework called No-More-Sliding-Window-Net (NMSW-Net), which closely resembles the segmentation protocols used by human radiologists described above. As illustrated in Fig 1, NMSW-Net replaces the costly SW inference method that applies the same compute resources across all patches with a differential patch sampling module that picks only a handful of patches with higher importance. NMSW-Net aggregates the predictions from the selected patches with low-res global prediction to produce the final full-res whole-volume prediction.

Specifically, NMSW-Net operates through a three-step process: (1) **Global Prediction:** A global model processes a low-resolution whole-slide volume, generating two outputs: a coarse global prediction and a discrete probability distribution that indicates the likelihood of each region enhancing the final prediction score when aggregated with the global prediction. (2) **Patch Selection and Prediction:** High-resolution patches are selected based on location vectors sampled from the discrete probability distribution using our proposed differentiable top-K sampling module. These selected patches are then processed by a local model to generate granular local predictions. (3) **Final Aggregation:** The coarse global prediction is combined with the top-K patch predictions through our aggregation module to produce the final prediction.

We emphasize that NMSW-Net is not a new segmentation model but a framework designed to enhance the computational efficiency of existing 3D medical image segmentation models. NMSW-Net can be integrated with any 3D model that previously employed SW. Across evaluations on three multi-organ segmentation tasks using three different backbone models, NMSW-Net consistently achieves competitive segmentation

performance, and in some cases even surpasses the SW baseline, while reducing computational cost by 90%.

## G. Contribution

Our contributions are summarized as follows:

- For the first time in the field, we propose an end-to-end trainable framework for whole-volume 3D segmentation, called NMSW-Net.
- NMSW-Net eliminates the need for expensive SW inference by implementing a differentiable top-K patch sampling technique that selects only the patches most likely to enhance segmentation accuracy.
- NMSW-Net learns to leverage coarse global predictions when patch prediction alone is insufficient.
- NMSW-Net consistently achieves competitive segmentation performance, and in some cases even surpasses the SW baseline, while reducing computational cost by 90%.

## II. RELATED STUDIES

### A. Practice of Sliding Window Inference in 3D model

SW has become the dominant approach to managing the high memory demands of 3D medical image segmentation in nearly all newly proposed models [9], [12], [13]. Even recent efforts to improve the efficiency of 3D segmentation models focus primarily on optimizing the backbone network [11], [14], [15], while relying on SW during inference.

Moreover, patch-based methods are widely adopted across various applications beyond 3D segmentation. Patch-based inference has proven to be effective but computationally expensive, for example, in computational pathology for whole-slide image analysis [16], [17] and mammogram classification [18].

Thus, while we present our approach as a solution to address the limitation of SW in 3D segmentation, it can tackle other mega- or gigapixel problems with minor modifications.

### B. Attempts to Reduce Computation Cost of 3D model

As aforementioned, most of recent efforts to improve the efficiency of 3D segmentation models focus primarily on optimizing the backbone architecture, while maintaining patch-based training, with only a few studies that attempt to reduce computational costs with efficient sampling strategy but with obvious scaling issues.

1) *Optimizing Backbone Architecture*: [11] addresses the computational complexity of the self-attention module by introducing a set of smaller attention modules, where each module processes a reduced number of tokens. The outputs of these resized tokens are then concatenated to restore the original token count. [19] replaces the standard multi-channel convolutions with channel-wise convolutions or  $1 \times 1$  convolutions. [20] uses knowledge distillation to supervise the training of a small student model with a large teacher model. Our proposed approach can be added on top of these lightweight models to make the inference cost even cheaper and faster.

2) *Optimizing Inference Strategy*: Though not explicitly mentioned in the literature, the following works have the potential to replace SW in 3D segmentation, but with some notable scaling issues.

Mask R-CNN [21] is a two-stage instance segmentation model that initially identifies ROI bounding boxes, followed by segmentation within the chosen ROIs. A low-resolution input could potentially be used in the initial region proposal stage. However, as noted in the article, the proposed ROIs frequently overlap substantially, thus a high number (300 to 1000) of crops should proceed to the segmentation stage for optimal results, potentially leading to even slower inference speed than SW.

Likewise, [22] proposes a two-step model where the first stage estimates a deformed grid from a low-resolution input, and the second stage uses this grid for resampling [23] the high-resolution input in an end-to-end differentiable manner. However, when applied to segmentation tasks, the image re-sampled from the learned grid can lead to information loss due to imprecise intensity interpolation, resulting in sub-optimal segmentation performance, when the prediction is mapped back to a uniform grid.

[24] proposes using Deep Q Learning [25] to allow a reinforcement learning (RL) agent to iteratively update a bounding box through a finite action space (e.g., zoom, shift). The reward is based on the overlap between the proposed bounding box and the ground truth mask. The updated bounding box is then used to crop a region for segmentation. Nevertheless, due to the iterative update procedure that involves treating a 3D volume as a state, this method is computationally inefficient and struggles with scalability for multi-organ tasks.

### C. Differentiable Patch Sampling in Computer Vision

While the use of a smart patch selection module instead of random patch training with SW may seem like a trivial solution that many have considered in the past, the non-differentiable nature of the sampling operation has been the key limiting factor in deep learning application.

In recent years, several methods have been proposed to make sampling operations differentiable. One of the earliest approaches to achieving differentiable sampling in deep learning was introduced by Kingma and Welling [26], who applied the reparameterization trick to a normal distribution, enabling backpropagation through stochastic nodes in neural networks.

Reparameterization trick was further explored by Maddison et al. [27] and Jang et al. [28], extending differentiability to any finite discrete distribution. Their approach used the Gumbel-Max trick [29], [30] which detaches a stochastic node from the rest of learnable deterministic nodes, and replaced the discrete argmax operation with temperature annealed softmax. Besides the reparameterization trick introduced, other approaches enabling learning through stochastic sampling include optimal transport [31], perturbed optimization [32], and Monte Carlo approximation [33].

Few studies have applied differentiable sampling techniques for importance-based patch sampling [34], [35], primarily targeting high-resolution 2D classification tasks. In contrast,

our proposed approach is specifically designed for 3D medical image segmentation, which presents additional challenges due to the high spatial resolution, small batch training, and the need to integrate coarse global predictions in the regions where predicted patches do not cover.

### III. METHOD

#### A. NMSW Overview

As shown in Fig. 2, unlike conventional patch-based training, which processes a batch of patches randomly sampled from a 3D full resolution scan, NMSW-Net takes the entire scan,  $\mathbf{x}_{\text{high}} \in \mathbb{R}^{H \times W \times D}$ , as input. In the model,  $\mathbf{x}_{\text{high}}$  is mapped to a downsized scan  $\mathbf{x}_{\text{low}} \in \mathbb{R}^{H' \times W' \times D'}$  and a list of overlapping patches sampled at a regular interval  $\mathbf{X}_{\text{patch}} = [\mathbf{x}_{\text{patch}}^{(1)}, \mathbf{x}_{\text{patch}}^{(2)}, \dots, \mathbf{x}_{\text{patch}}^{(N)}] \in \mathbb{R}^{N \times H_p \times W_p \times D_p}$ , where  $N$  is the total number of patches<sup>1</sup>.

The global backbone  $f_g$ , a generic semantic segmentation model, takes  $\mathbf{x}_{\text{low}}$  and produces two outputs: 1) a coarse global prediction  $\hat{\mathbf{y}}_{\text{low}} \in [0, 1]^{C \times H_l \times W_l \times D_l}$  and 2) a discrete pdf  $p(\mathbf{z}|\mathbf{x}_{\text{low}}) \in [0, 1]^N$  (represented as 2D in Fig 2 for better visualization) which estimates the importance of individual patches in contributing to the accuracy of the final segmentation map  $\hat{\mathbf{y}}_{\text{high}}$ .

$K$  important patch locations,  $\{\mathbf{z}^{(k)} \in [0, 1]^N\}_{k=1}^K$ , are sampled from  $p(\mathbf{z}|\mathbf{x}_{\text{low}})$  without replacement using the **Differentiable Top-K** block. Subsequently,  $K$  important patches,  $\{\mathbf{x}_{\text{patch}}^{(k*)}\}_{k=1}^K$ , are chosen from  $[\mathbf{x}_{\text{patch}}^{(1)}, \mathbf{x}_{\text{patch}}^{(2)}, \dots, \mathbf{x}_{\text{patch}}^{(N)}]$  based on  $\{\mathbf{z}^{(k)}\}_{k=1}^K$ .

The selected patches are mapped to patch predictions,  $\{\hat{\mathbf{y}}_{\text{patch}}^{(k)} \in [0, 1]^{C \times H_p \times W_p \times D_p}\}_{k=1}^K$ , using another semantic segmentation model at the patch level, denoted as  $f_i$ . The global and local models do not share weights and are not required to have identical model architectures. As the final step, the **Aggregation** block combines  $\hat{\mathbf{y}}_{\text{low}}$  with  $\{\hat{\mathbf{y}}_{\text{patch}}^{(k)}\}$  to produce the final whole-volume prediction,  $\hat{\mathbf{y}}_{\text{high}}$ .

All modules in NMSW are differentiable, enabling end-to-end gradient-based training to produce the whole-volume prediction. Thus NMSW eliminates the need for heuristic methods like SW to convert patch predictions into a full-volume prediction.

#### B. Blocks

1) **Differentiable Top-K**: Training a stochastic module like **Differentiable Top-K** is challenging due to two non-differentiable operations: (1) the random sampling operation and (2) the categorical nature of the samples. To address the non-differentiability problem, we introduce a modified version of Reparameterizable Subset Sampling algorithm [42], which generalizes the Gumbel-Softmax trick to a Top-K sampling scenario.

<sup>1</sup>The size of  $N$  is computed as  $N = N_h \cdot N_w \cdot N_d$ , where  $N_h$ ,  $N_w$ , and  $N_d$  are the patch numbers at corresponding dimension. For instance, in dimension  $D$ ,  $N_d$  is given by  $N_d = \lfloor \frac{D - D_p}{D_p \cdot o_d} \rfloor + 1$ , where,  $r_d$  is the downsampling ratio, and  $o_d$  is the overlapping ratio.

**Gumbel-Softmax** [27], [28]: We begin by introducing Gumbel-Softmax, which proposes reparameterizable continuous relaxations of a categorical distribution. Given a categorical distribution  $p(\mathbf{z})$ , where the probability of the  $n$ -th outcome is  $p(\mathbf{z} = n) = \pi_n$ , Gumbel-Softmax approximates the sampling operation ( $z \sim p(\mathbf{z})$ ) as:

$$\mathbf{z}_{\text{soft\_hot}} = [y_1, y_2, \dots, y_N], \quad y_n = \sigma_\tau(\log(\pi_n) + g_n), \quad (1)$$

where taking  $\text{argmax}$  on  $\mathbf{z}_{\text{soft\_hot}}$  gives  $z$ .  $g_i \sim \text{Gumbel}(0, 1)$  is a sample from the Gumbel distribution with  $\mu = 0$  and  $\beta = 1$ .<sup>2</sup> The  $\sigma_\tau$  is a softmax function with a temperature parameter  $\tau \in [0, \infty]$ , defined as:

$$\sigma_\tau(x_n) = \frac{\exp((\log(x_n) + g_n)/\tau)}{\sum_{m=1}^N \exp((\log(x_m) + g_m)/\tau)}. \quad (2)$$

As  $\tau$  approaches 0, the Gumbel-Softmax estimator approximates the target categorical distribution  $p(\mathbf{z})$ .

**Differentiable Top-K**: generalizes the Gumbel-Softmax estimator to draw Top-K samples without replacement. Unlike Gumbel-Softmax which has a fixed distribution  $p(\mathbf{z})$  throughout sampling, **Differentiable Top-K** (Fig 3(a)) masks the probabilities of previously sampled outcomes. For instance, the  $k$ -th random sample,  $\mathbf{z}_{\text{soft\_hot}}^{(k)}$ , is defined as:

$$\mathbf{z}_{\text{soft\_hot}}^{(k)} = [y_1^{(k)}, y_2^{(k)}, \dots, y_N^{(k)}], \quad y_i^{(k)} = \sigma_\tau(\log(\pi_i^{(k)}) + g_i), \quad (3)$$

where

$$\pi_i^{(k)} = \begin{cases} \pi_i^{(k)} & i \neq \text{argmax}(\mathbf{z}_{\text{soft\_hot}}^{(k-1)}), \\ 0 & \text{otherwise,} \end{cases} \quad (4)$$

and for the initial case,  $\pi_i^{(1)} = \pi_i$ .

Our application strictly requires the sampled variable to be one\_hot rather than soft\_hot, as artifacts from other patches may otherwise contaminate the extracted patches. While the Straight-Through (ST)<sup>3</sup> estimation addresses this by enabling one\_hot behavior in the forward pass and soft\_hot behavior in the backward pass, it introduces huge gradient bias especially during the early training stage when the probability is not saturated. To mitigate this, we propose an adjustment to ST by scaling the one\_hot samples with their corresponding soft\_hot values:  $\mathbf{z}^{(k)} = \mathbf{z}_{\text{one\_hot}}^{(k)} \cdot \mathbf{z}_{\text{soft\_hot}}^{(k)}$ . This adjustment accelerates convergence by reducing the gradient bias.

Top-K patches are extracted from the candidate patches via a simple inner product:

$$\mathbf{x}_{\text{patch}}^{k*} = \langle \mathbf{z}^{(k)}, \mathbf{X}_{\text{patch}} \rangle. \quad (5)$$

Since the maximum value of  $\mathbf{z}^{(k)}$  lies within the interval  $[0, 1]$ , the intensity of the extracted patches is proportionally affected, as illustrated by the colored output patches in Fig 3(a).

<sup>2</sup>Sampling from the Gumbel distribution can be simulated by transforming uniform samples:  $g = -\log(-\log(u))$ ,  $u \sim U(0, 1)$ .

<sup>3</sup>In pytorch ST is done with a simple gradient detach  $\mathbf{z}_{\text{one\_hot}} := \mathbf{z}_{\text{soft\_hot}} \cdot \text{detach}() + \mathbf{z}_{\text{one\_hot}} \cdot \text{detach}() - \mathbf{z}_{\text{soft\_hot}}$

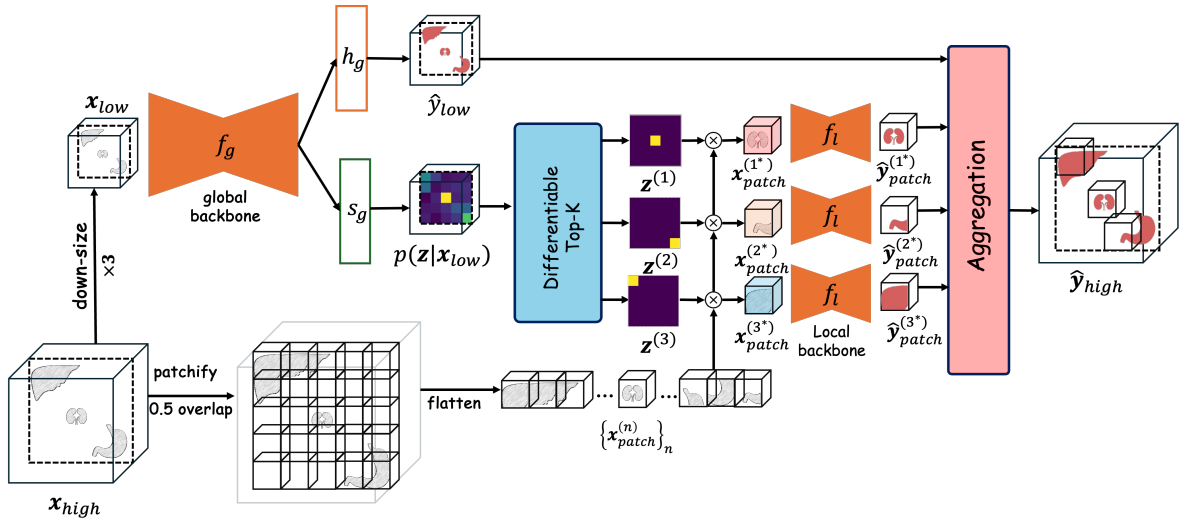


Fig. 2. NMSW-Net takes the full resolution scan  $x_{high}$  as an input. Global backbone  $f_g$  maps a downsized scan  $x_{low}$  to a coarse global prediction  $\hat{y}_{low}$  and a discrete probability distribution  $p(z|x_{low})$  that measures the importance of regions in the scan.  $K$  regions highlights  $\{z^{(k)}\}$  are sampled from  $p(z|x_{low})$  with **Differentiable\_Top-K** block. Region highlights are used to sample the patches in the corresponding region  $\{x_{patch}^{(k)}\}$ . Sampled patches are mapped to patch predictions  $\{\hat{y}_{patch}^{(k)}\}$  with local backbone  $f_l$ .  $\{\hat{y}_{patch}^{(k)}\}$  and  $\hat{y}_{low}$  are combined in **Aggregation** block to produce the final Whole-Body prediction  $\hat{y}_{high}$ .

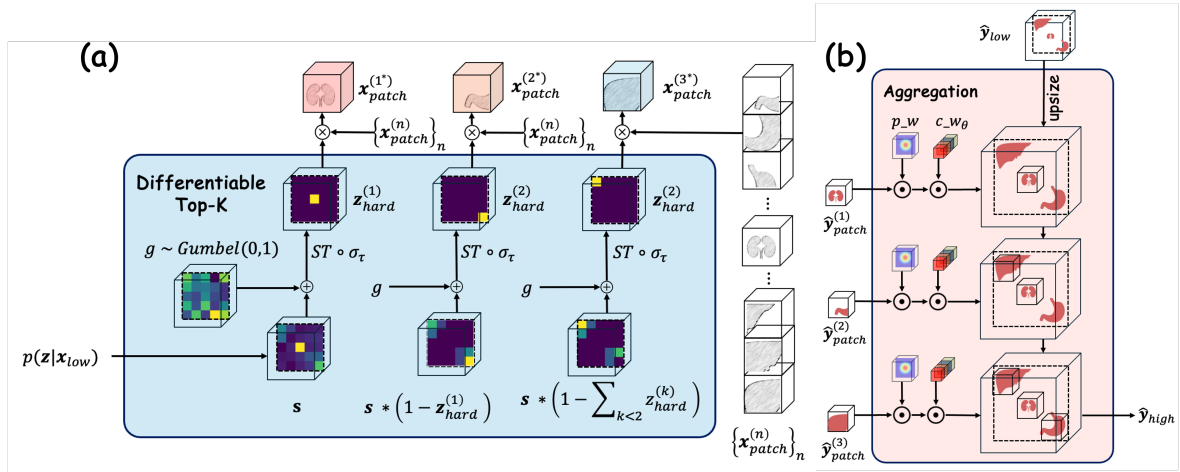


Fig. 3. Illustration of (a) **Differentiable Top-K Block** and (b) **Aggregation Block**. The **Differentiable Top-K** block selects the top-K important patches  $\{z^{(k)}\}$  from  $p(z|x_{low})$  using the Gumbel-Top-K trick, a differentiable extension of Gumbel-Softmax. This method iteratively modifies the distribution  $p(z|x_{low})$  by masking the probability of previously sampled region. The **Aggregation** block combines the global prediction  $\hat{y}_{low}$  and local patch predictions  $\{\hat{y}_{patch}^{(k)}\}$  to generate the final prediction  $\hat{y}_{high}$ . Local predictions are weighted by  $p_w$  (overlap adjustment) and  $c_w_\theta$  (relative importance) before aggregation with the upscaled global prediction.

2) **Aggregation**: Given a set of patch predictions  $\{\hat{y}^{(k)}\}$  from the selected Top-K patches and the coarse global prediction  $x_{global}$ . **Aggregation** block merges the two predictions into the final whole scan prediction  $\hat{y}_{high}$  in a fully differentiable way.

A naive approach would be to simply paste or overwrite the predicted patches onto the upscaled coarse prediction. However, this approach could lead to suboptimal predictions for two reasons: (1) Predicted patches often have overlapping areas, and merely pasting them disregards contributions from other patches in these regions. (2) A simple overwrite assumes that patch predictions are always more accurate than the coarse prediction, which may not hold true, especially for objects that rely on global features.

The **Aggregation** block 3(b) addresses the two biases present in the naive approach. Before adding the patches to the upscaled coarse prediction, each patch is multiplied by a patch weight,  $p_w \in [0, 1]^{P_h \times P_w \times P_d}$ , which is a discretized Gaussian distribution with  $\mu = 0$  and  $\sigma = 0.125$ . This multiplication enables the model to blend the patches smoothly in the overlapping regions.<sup>4</sup> To have a weighted prediction between the global and patch predictions, we also introduce a learnable class weight  $c_w_\theta \in [0, 1]^C$ . This allows the model to leverage global predictions for specific organs when necessary. A predicted patch is added to the upscaled global prediction

<sup>4</sup>Although it is possible to make  $p_w$  learnable, our experiments did not show significant improvement in performance

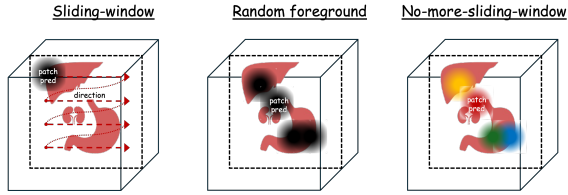


Fig. 4. We evaluate NMSW-Net in comparison to SW and RF inference techniques. The key advantage of NMSW over RF is its ability to rank patch importance, a feature absent in RF. This ranking capability is visually illustrated in the figure, where patches are highlighted in different colors to reflect their relative importance.

in the corresponding region  $\Omega(k)$  by :

$$\hat{\mathbf{y}}_{\Omega(k)} := \sigma(c_{-w\theta}) \cdot p_{-w} \cdot \hat{\mathbf{y}}_{\text{patch}}^{(k)} + (1 - \sigma(c_{-w\theta})) \cdot \hat{\mathbf{y}}_{\Omega(k)} \quad (6)$$

### C. Loss Function

We apply the conventional soft-Dice combined with cross-entropy to three model predictions:  $\hat{\mathbf{y}}_{\text{low}}$ ,  $\{\hat{\mathbf{y}}_{\text{patch}}^{(k)}\}_{k=1}^K$ , and  $\hat{\mathbf{y}}_{\text{high}}$ . To encourage the model to explore diverse regions during training, we introduce an entropy regularization term on the patch selection distribution  $p(\mathbf{z} | \mathbf{x}_{\text{low}})$ . The total loss function is defined as:

$$L_{\text{total}} = L_{\text{dice}}(\mathbf{y}_{\text{low}}, \hat{\mathbf{y}}_{\text{low}}) + L_{\text{dice}}(\mathbf{y}_{\text{high}}, \hat{\mathbf{y}}_{\text{high}}) + \frac{1}{K} \sum_{k=1}^K L_{\text{dice}}(\mathbf{y}_{\text{patch}}^{(k)}, \hat{\mathbf{y}}_{\text{patch}}^{(k)}) + \lambda \mathcal{H}(p(\mathbf{z} | \mathbf{x}_{\text{low}})), \quad (7)$$

where  $\mathbf{y}_{\text{low}}$ ,  $\{\mathbf{y}_{\text{patch}}^{(k)}\}_{k=1}^K$ , and  $\mathbf{y}_{\text{high}}$  represent the ground-truth labels corresponding to the respective predictions,  $\mathcal{H}$  denotes the entropy function, and  $\lambda \in [0, 1]$  is a hyperparameter.

## IV. EXPERIMENTS

### A. Comparative Baseline Inference Techniques

Fig 4 illustrates the two baseline inference SW and Random Foreground (RF)—which are compared with our NMSW-Net.

1) *Sliding Window*: SW is the most commonly used inference technique, relying solely on a local patch-based model. It produces the final volume prediction by scanning the volume at a regular interval.

2) *Random Foreground*: RF closely resembles NMSW, with two key distinctions: 1) the sampling strategy, and 2) the method of aggregation. Similar to NMSW, RF samples patches containing objects of interest. However, it does not rank their importance; all patches are equally likely to be selected if they contain objects of interest. Furthermore, the class weights  $c_{-w\theta}$  in the *Aggregation* block are set to a high value, reflecting the common assumption that local predictions generally outperform global predictions.

### B. Backbones

For the local network, we evaluate three popular backbones for medical image segmentation: UNet [37], MedNext [38], and Swin-UNETR [12], while using UNet as the global network for computational efficiency.

1) *UNet*: We employ down- and up-sampling blocks with channel sizes [32, 64, 128, 256, 320] and a bottleneck block of 320 channels.

2) *MedNext*: MedNext uses the convolutional blocks as proposed in ConvNext [39]. ConvNext employs large convolutional kernels and grouped convolutions to optimize memory usage. We use the medium MedNext configuration, featuring down- and up-sampling blocks with channel sizes [32, 64, 128, 256, 512] and a bottleneck of 512 channels.

3) *Swin-UNETR*: Swin-UNETR fuses Swin Transformer [40] and standard convolutional blocks. The Swin Transformer has an embedding size of 24 with a kernel size of 7. It consists of 8 Swin Transformer blocks, with the number of attention heads progressively increasing from 3 to 24.

Please see our code for further details of the backbone architectures.

### C. Datasets

Each combination of the aforementioned segmentation backbones and inference techniques is trained on two multi-organ segmentation datasets: WORD [1] and TotalSegmentator [10]. We did not evaluate NMSW on datasets with limited annotated classes, such as tumor or single-organ prediction tasks, because, while NMSW is applicable to these scenarios, the problem would likely simplify our top-K patch sampling module to a boring single-patch sampling module.

1) *WORD*: WORD consists of 150 CT scans, each annotated with 16 organs. Each scan contains 159–330 slices with a resolution of  $512 \times 512$  pixels and an in-plane spacing of  $0.976 \times 0.976$  mm. We preprocess the data to normalize the spacing to  $1 \times 1 \times 3$  mm, resulting in a shape at the 99.5% percentile of  $512 \times 512 \times 336$ .

2) *TotalSegmentator*: TotalSegmentator contains 1,204 CT scans, annotated with 104 organs. From the full set of labels, we select two subsets: Organ and Vertebrae. TotalSegmentator exhibits considerable shape variability, with dimensions ranging from  $47 \times 48 \times 29$  to  $499 \times 430 \times 852$ . We normalize the spacing to  $1.5 \times 1.5 \times 1.5$  mm, resulting in a shape at the 99.5% percentile of  $373 \times 333 \times 644$ .

### D. Training Details

For both baseline inference techniques and our proposed NMSW-Net, we fixed the overlap ratio between patches at 50% and the patch size at  $128 \times 128 \times 128$ . The down-size rate of global input is set to  $3 \times 3 \times 3$  for WORD and  $3 \times 3 \times 4$  for TotalSegmentator. We trained for 300 epochs, with 300 iterations per epoch. During training, for the baseline approaches, the batch size was set to 4, while for NMSW, we sampled 3 top-k patches and 1 random patch per iteration, resulting in the same number of patches as baseline approaches. For the loss in Eq 7, the weights of soft-Dice and cross-entropy is set to 0.8 and 0.2, respectively. The entropy weight  $\lambda$  is set to 0.0001.

We employed the AdamW optimizer [41] with a learning rate of  $3e-4$  and weight decay of  $1e-5$ , along with a cosine

TABLE I

ACCURACY AND EFFICIENCY COMPARISON BETWEEN OUR PROPOSED NMSW AND TWO BASELINE METHODS, SLIDING-WINDOW AND RANDOM-FOREGROUND, ACROSS THREE SEGMENTATION TASKS: WORD, TOTALSEGMENTATOR ORGAN (TOTALORGAN), AND TOTALSEGMENTATOR VERTEBRAE (TOTALVERTEBRAE).  $k$  REPRESENTS THE NUMBER OF PATCHES USED FOR EACH INFERENCE. THE SPEED OF RF IS OMITTED, AS ITS NETWORK STRUCTURE IS NEARLY IDENTICAL TO NMSW, THUS GIVING IDENTICAL INFERENCE SPEED. THE COMPUTED SPEED AND GFLOPS ASSUMES AN INPUT OF SIZE  $1 \times 480 \times 480 \times 480$  WITH 14 OUTPUT CHANNELS.

Model type	Dataset									Inference Speed			
	Word			TotalOrgan			TotalVertebrae			GPU	CPU	Flops (T)	Model Size (M)
	HD <sub>95</sub> ↓	DSC ↑	NSD ↑	HD <sub>95</sub> ↓	DSC ↑	NSD ↑	HD <sub>95</sub> ↓	DSC ↑	NSD ↑				
<b>UNet</b>													
Sliding-window	5.79	0.853	0.906	5.08	0.859	0.869	2.19	0.872	0.932	3.21	83.0	51.3	26.5
Random-foreground (k=5)	7.62	0.789	0.805	6.36	0.803	0.803	5.00	0.701	0.765	-	-	-	-
Random-foreground (k=30)	6.61	0.830	0.870	6.65	0.828	0.825	4.09	0.787	0.851	-	-	-	-
NMSW (k=5)	7.10	0.812	0.839	5.54	0.856	0.864	2.84	0.822	0.875	1.32	15.6	1.04	-
NMSW (k=30)	5.86	0.850	0.896	4.65	0.875	0.895	2.92	0.846	0.885	1.50	29.5	4.80	53.0
<b>Swin-unetr</b>													
Sliding-window	5.77	0.848	0.897	6.97	0.836	0.838	3.23	0.841	0.897	14.3	708	68.7	15.5
Random-foreground (k=5)	7.90	0.781	0.795	7.22	0.782	0.785	5.74	0.671	0.741	-	-	-	-
Random-foreground (k=30)	7.24	0.824	0.862	8.80	0.806	0.786	5.84	0.747	0.803	-	-	-	-
NMSW (k=5)	7.08	0.818	0.846	5.13	0.841	0.853	4.18	0.752	0.833	1.71	29.7	1.29	-
NMSW (k=30)	6.18	0.839	0.882	3.52	0.889	0.915	-	-	-	3.28	115	6.30	42.0
<b>MedNext</b>													
Sliding-window	5.10	0.860	0.913	4.10	0.885	0.901	2.12	0.903	0.942	19.0	1720	87.5	17.5
Random-foreground (k=5)	7.65	0.789	0.802	5.89	0.816	0.821	5.19	0.767	0.699	-	-	-	-
Random-foreground (k=30)	5.85	0.848	0.896	5.53	0.857	0.862	4.19	0.809	0.855	-	-	-	-
NMSW (k=5)	6.21	0.824	0.864	5.15	0.847	0.853	2.49	0.874	0.931	2.64	51.5	1.56	-
NMSW (k=30)	5.29	0.853	0.909	3.52	0.889	0.915	2.32	0.900	0.949	4.31	231.0	7.95	44.1

annealing learning rate scheduler that reaches the maximum learning rate at 20% of the training iterations.

The data augmentation pipeline includes intensity scaling, affine transformations (translation, rotation, scaling), Gaussian noise and smoothing, intensity scaling, contrast adjustments, low-resolution simulations, and grid distortion.

## V. RESULTS

### A. Trade-off between accuracy and efficiency

Table I compares NMSW-Net against two baselines—SW and RF—in terms of segmentation performance and computational efficiency. The observed trend is consistent throughout: although NMSW-Net doubles the model size due to the inclusion of an additional global segmentation model, it achieves significantly improved computational efficiency while maintaining competitive segmentation performance when the number of sampled patches is 30 ( $k = 30$ ). While the RF baseline is equally efficient, its patch sampling does not necessarily target regions where the global prediction is most deficient, resulting in a significantly smaller accuracy boost from the sampled patches.

In terms of floating-point operations per second (FLOPs), which correlate with the model’s overall energy consumption, NMSW-Net uses approximately 90% fewer FLOPs compared to SW. Additionally, NMSW-Net is, on average, about 4× faster in both CPU (Intel Xeon Gold) and GPU (H100) environments. Notably, the speed improvement becomes more pronounced as the complexity of the backbone model increases. This is because, unlike SW, NMSW-Net incorporates additional computations from the global segmentation model, but their impact diminishes as the local backbone’s complexity increases.

It is worth mentioning that NMSW-Net outperforms SW in the TotalSegmentatorOrgan task in terms of overall accuracy.

We hypothesize that the learnable patch sampling module in NMSW-Net not only improves computational efficiency but also enhances accuracy by focusing on regions where the model underperforms during training. Thus, our **Differentiable Top-K** module can be viewed as a special kind of active learning algorithm that samples data points where the model performs poorly. In our case, the data points are patches. Further investigation of this hypothesis is left for future research.

### B. Evaluation of the Learned Class Weight

The class weight  $c_{\mathbf{w}_\theta}$  adjusts the importance of predictions in regions where global and patch predictions overlap. As shown in Fig. 7,  $\sigma(c_{\mathbf{w}_\theta})$  exhibits a consistent trend across various backbones trained on the WORD task. Models generally assign higher weights (above 0.5) to patch predictions, particularly for small or complex organs (e.g., pancreas, duodenum, colon, intestine), while slightly lower weights are given to more isolated or less complex structures (e.g., femur, rectum). Interestingly, stronger backbones like MedNextMedium emphasize local predictions more heavily, effectively ignoring global predictions when the local model is powerful.

### C. Evaluation of sampled Top-K patches

Fig. 5 illustrates the evolution of the patch sampling distribution,  $p(\mathbf{z}|\mathbf{x}_{\text{low}})$ , during training. Initially, the distribution is nearly random, with sampled regions (highlighted as red rectangles) scattered indiscriminately, failing to focus on foreground areas. Midway through training, the distribution begins to concentrate on foreground regions, but the sampled patches exhibit significant overlap, which is suboptimal for improving accuracy. By the end of training, the distribution not only targets foreground regions but are more well spread with less

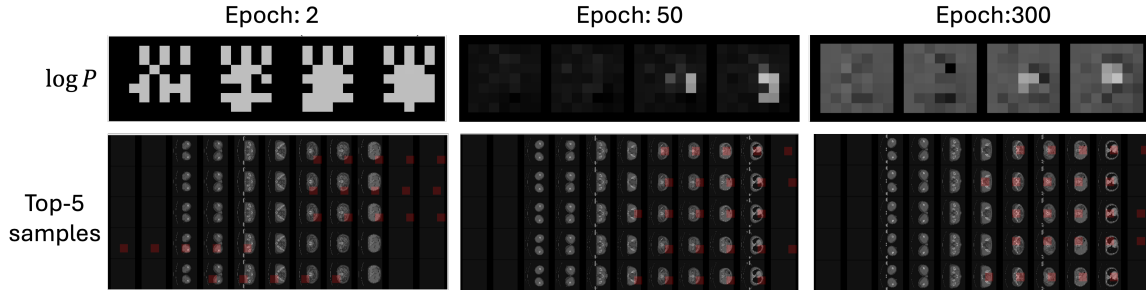


Fig. 5. the evolution of the patch sampling distribution  $p(z|x_{low})$  during training. Initially, sampling is random, ignoring foreground areas. Midway, the distribution focuses on the foreground but with significant overlap. By the end, the distribution highlights diverse foreground regions with minimal overlap.

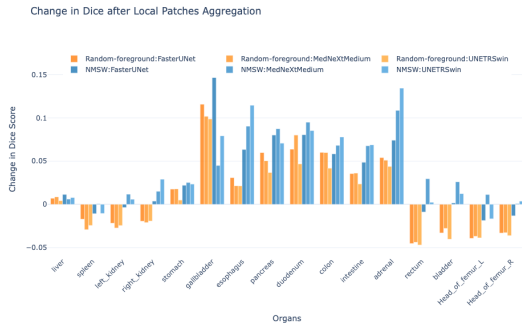


Fig. 6. Dice score improvement achieved by our proposed Top-K sampling block versus the RF sampling strategy when the global prediction is supplemented with the top-5 patches.

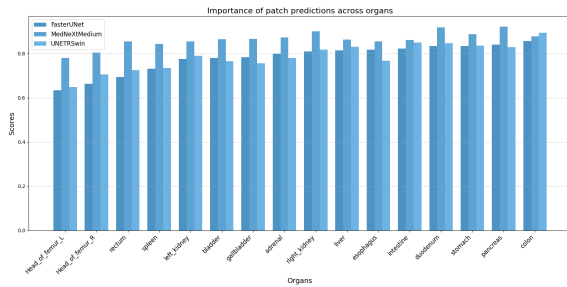


Fig. 7. Class weights learned by NMSW-Net. The model assigns higher weights (above 0.5) to patch predictions, particularly for small or complex organs (e.g., pancreas, duodenum, colon, intestine), while slightly lower weights are given to more isolated or less complex structures (e.g., femur, rectum).

overlap. This improvement is driven by the entropy term in the loss function, which encourages exploration of diverse regions and reduces overlap among sampled patches.

Fig. 6 compares the Dice score improvement achieved by our proposed Top-K sampling block and the RF sampling strategy when the global prediction is supplemented with the top-5 patches. While both RF and NMSW-Net enhance performance, NMSW-Net delivers a greater improvement across all organs. This indicates that the learned distribution is dynamic, adapting to compensate for organs where the global model underperforms, rather than focusing on a specific organ. Consequently, our sampling module is more than a simple foreground sampler with minimal overlap; it intelligently targets areas requiring enhancement.

## VI. CONCLUSION & DISCUSSION & FUTURE WORKS

Segmentation models, like those in other fields, have become increasingly slower, larger, and more computationally expensive. While prior efforts to improve efficiency have primarily focused on simplifying backbone architectures, NMSW takes a novel approach by replacing the time-consuming sliding-window inference in 3D segmentation tasks with dynamic patch sampling. NMSW is model-agnostic and can be seamlessly integrated into existing 3D segmentation architectures with minimal computational overhead.

In evaluations across various tasks and segmentation backbones, NMSW demonstrates substantial computational savings—achieving up to 90% lower FLOPs and  $4\times$  faster inference on GPUs (or  $5\times$  faster on CPUs)—while maintaining, and occasionally surpassing, the performance of costly SW inference.

While these results are promising, a few challenges remain to be addressed before the community can completely move away from SW:

- **Training Speed:** Although NMSW accelerates inference, its training is slower due to the sequential dependency between global and local computations. The local network remains idle until it receives patches sampled by the global network, limiting parallelization. Future research could explore strategies to improve training efficiency by reducing this bottleneck.
- **Task Expansion:** We tested NMSW exclusively on instance segmentation tasks. Extending its applicability to foundation vision-language models, expanding the applicability to open-vocabulary segmentation tasks.
- **Top-K Sampling:** The current Top-K sampling module selects patches *without replacement*. However, this approach is sub-optimal if the object of interest is small enough to fit within a single patch. The remaining  $k - 1$  patches are redundant background patches. Future work could explore relaxing this restriction by enabling *sampling with replacement*.

In conclusion, NMSW-Net presents a novel approach to achieving a more compute-efficient 3D segmentation model through attention-driven patch sampling. This method stands apart from conventional approaches, which typically rely on architectural modifications to segmentation backbones that are often task-specific and non-scalable. We hope that NMSW-Net



serves as a wake-up call for the community, inspiring further exploration of dynamic sampling techniques as a pathway toward more efficient 3D medical image segmentation.

## VII. ACKNOWLEDGMENT

The preferred spelling of the word “acknowledgment” in American English is without an “e” after the “g.” Use the singular heading even if you have many acknowledgments. Avoid expressions such as “One of us (S.B.A.) would like to thank . . . .” Instead, write “F. A. Author thanks . . . .” In most cases, sponsor and financial support acknowledgments are placed in the unnumbered footnote on the first page, not here.

## REFERENCES

- [1] Luo, X., Liao, W., Xiao, J., Chen, J., Song, T., Zhang, X., Li, K., Metaxas, D., Wang, G. & Zhang, S. WORD: A large scale dataset, benchmark and clinical applicable study for abdominal organ segmentation from CT image. *Medical Image Analysis*. **82** pp. 102642 (2022,11), <http://dx.doi.org/10.1016/j.media.2022.102642>
- [2] Avesta, A., Hossain, S., Lin, M., Aboian, M., Krumholz, H. & Aneja, S. Comparing 3D, 2.5 D, and 2D approaches to brain image auto-segmentation. *Bioengineering*. **10**, 181 (2023)
- [3] LeCun, Y., Bottou, L., Bengio, Y. & Haffner, P. Gradient-based learning applied to document recognition. *Proceedings Of The IEEE*. **86**, 2278-2324 (1998)
- [4] Vaswani, A. Attention is all you need. *Advances In Neural Information Processing Systems*. (2017)
- [5] Gu, A. & Dao, T. Mamba: Linear-time sequence modeling with selective state spaces. *ArXiv Preprint arXiv:2312.00752*. (2023)
- [6] Chellapilla, K., Puri, S. & Simard, P. High performance convolutional neural networks for document processing. *Tenth International Workshop On Frontiers In Handwriting Recognition*. (2006)
- [7] Winograd, S. Arithmetic complexity of computations. (Siam,1980)
- [8] Dosovitskiy, A. An image is worth 16x16 words: Transformers for image recognition at scale. *ArXiv Preprint arXiv:2010.11929*. (2020)
- [9] Isensee, F., Jaeger, P., Kohl, S., Petersen, J. & Maier-Hein, K. nnU-Net: a self-configuring method for deep learning-based biomedical image segmentation. *Nature Methods*. **18**, 203-211 (2021)
- [10] Wasserthal, J., Breit, H., Meyer, M., Pradella, M., Hinck, D., Sauter, A., Heye, T., Boll, D., Cyriac, J., Yang, S. & Others TotalSegmentator: robust segmentation of 104 anatomic structures in CT images. *Radiology: Artificial Intelligence*. **5** (2023)
- [11] Perera, S., Navard, P. & Yilmaz, A. SegFormer3D: an Efficient Transformer for 3D Medical Image Segmentation. *Proceedings Of The IEEE/CVF Conference On Computer Vision And Pattern Recognition*. pp. 4981-4988 (2024)
- [12] Hatamizadeh, A., Nath, V., Tang, Y., Yang, D., Roth, H. & Xu, D. Swin unetr: Swin transformers for semantic segmentation of brain tumors in mri images. *International MICCAI Brainlesion Workshop*. pp. 272-284 (2021)
- [13] Sekuboyina, A., Hussein, M., Bayat, A., Löffler, M., Liebl, H., Li, H., Tetteh, G., Kukačka, J., Payer, C., Štern, D. & Others VerSe: a vertebrae labelling and segmentation benchmark for multi-detector CT images. *Medical Image Analysis*. **73** pp. 102166 (2021)
- [14] Deng, Y., Hou, Y., Yan, J. & Zeng, D. ELU-Net: An Efficient and Lightweight U-Net for Medical Image Segmentation. *IEEE Access*. **10** pp. 35932-35941 (2022)
- [15] Qin, D., Bu, J., Liu, Z., Shen, X., Zhou, S., Gu, J., Wang, Z., Wu, L. & Dai, H. Efficient Medical Image Segmentation Based on Knowledge Distillation. *IEEE Transactions On Medical Imaging*. **40**, 3820-3831 (2021)
- [16] Lu, M., Williamson, D., Chen, T., Chen, R., Barbieri, M. & Mahmood, F. Data-efficient and weakly supervised computational pathology on whole-slide images. *Nature Biomedical Engineering*. **5**, 555-570 (2021)
- [17] Bae, K., Jeon, Y., Hwangbo, Y., Yoo, C., Han, N., Feng, M. & Others Data-Efficient Computational Pathology Platform for Faster and Cheaper Breast Cancer Subtype Identifications: Development of a Deep Learning Model. *JMIR Cancer*. **9**, e45547 (2023)
- [18] Lotter, W., Sorensen, G. & Cox, D. A multi-scale CNN and curriculum learning strategy for mammogram classification. *Deep Learning In Medical Image Analysis And Multimodal Learning For Clinical Decision Support: Third International Workshop, DLMIA 2017, And 7th International Workshop, ML-CDS 2017, Held In Conjunction With MICCAI 2017, Québec City, QC, Canada, September 14, Proceedings 3*. pp. 169-177 (2017)
- [19] Alalwan, N., Abozeid, A., ElHabshy, A. & Alzahrani, A. Efficient 3D deep learning model for medical image semantic segmentation. *Alexandria Engineering Journal*. **60**, 1231-1239 (2021)
- [20] Qin, D., Bu, J., Liu, Z., Shen, X., Zhou, S., Gu, J., Wang, Z., Wu, L. & Dai, H. Efficient medical image segmentation based on knowledge distillation. *IEEE Transactions On Medical Imaging*. **40**, 3820-3831 (2021)
- [21] He, K., Gkioxari, G., Dollár, P. & Girshick, R. Mask R-CNN. (2018), <https://arxiv.org/abs/1703.06870>
- [22] Recasens, A., Kellnhofer, P., Stent, S., Matusik, W. & Torralba, A. Learning to zoom: a saliency-based sampling layer for neural networks. *Proceedings Of The European Conference On Computer Vision (ECCV)*. pp. 51-66 (2018)
- [23] Jaderberg, M., Simonyan, K., Zisserman, A. & Others Spatial transformer networks. *Advances In Neural Information Processing Systems*. **28** (2015)
- [24] Man, Y., Huang, Y., Feng, J., Li, X. & Wu, F. Deep Q learning driven CT pancreas segmentation with geometry-aware U-Net. *IEEE Transactions On Medical Imaging*. **38**, 1971-1980 (2019)
- [25] Mnih, V. Playing atari with deep reinforcement learning. *ArXiv Preprint arXiv:1312.5602*. (2013)
- [26] Kingma, D. Auto-encoding variational bayes. *ArXiv Preprint arXiv:1312.6114*. (2013)
- [27] Maddison, C., Mnih, A. & Teh, Y. The concrete distribution: A continuous relaxation of discrete random variables. *ArXiv Preprint arXiv:1611.00712*. (2016)
- [28] Jang, E., Gu, S. & Poole, B. Categorical reparameterization with gumbel-softmax. *ArXiv Preprint arXiv:1611.01144*. (2016)
- [29] Gumbel, E. Statistical theory of extreme value and some practical applications. *Nat. Bur. Standards Appl. Math. Ser. 33*. (1954)
- [30] Maddison, C., Tarlow, D. & Minka, T. A\* sampling. *Advances In Neural Information Processing Systems*. **27** (2014)
- [31] Xie, Y., Dai, H., Chen, M., Dai, B., Zhao, T., Zha, H., Wei, W. & Pfister, T. Differentiable top-k with optimal transport. *Advances In Neural Information Processing Systems*. **33** pp. 20520-20531 (2020)
- [32] Berthet, Q., Blondel, M., Teboul, O., Cuturi, M., Vert, J. & Bach, F. Learning with differentiable perturbed optimizers. *Advances In Neural Information Processing Systems*. **33** pp. 9508-9519 (2020)
- [33] Paisley, J., Blei, D. & Jordan, M. Variational Bayesian Inference with Stochastic Search. (2012), <https://arxiv.org/abs/1206.6430>
- [34] Cordonnier, J., Mahendran, A., Dosovitskiy, A., Weissenborn, D., Uszkoreit, J. & Unterthiner, T. Differentiable patch selection for image recognition. *Proceedings Of The IEEE/CVF Conference On Computer Vision And Pattern Recognition*. pp. 2351-2360 (2021)
- [35] Katharopoulos, A. & Fleuret, F. Processing megapixel images with deep attention-sampling models. *International Conference On Machine Learning*. pp. 3282-3291 (2019)
- [36] Cardoso, M., Li, W., Brown, R., Ma, N., Kerfoot, E., Wang, Y., Murrey, B., Myronenko, A., Zhao, C., Yang, D. & Others Monai: An open-source framework for deep learning in healthcare. *ArXiv Preprint arXiv:2111.02701*. (2022)
- [37] Ronneberger, O., Fischer, P. & Brox, T. U-net: Convolutional networks for biomedical image segmentation. *Medical Image Computing And Computer-assisted Intervention-MICCAI 2015: 18th International Conference, Munich, Germany, October 5-9, 2015, Proceedings, Part III 18*. pp. 234-241 (2015)
- [38] Roy, S., Koehler, G., Ulrich, C., Baumgartner, M., Petersen, J., Isensee, F., Jaeger, P. & Maier-Hein, K. Mednext: transformer-driven scaling of convnets for medical image segmentation. *International Conference On Medical Image Computing And Computer-Assisted Intervention*. pp. 405-415 (2023)
- [39] Liu, Z., Mao, H., Wu, C., Feichtenhofer, C., Darrell, T. & Xie, S. A convnet for the 2020s. *Proceedings Of The IEEE/CVF Conference On Computer Vision And Pattern Recognition*. pp. 11976-11986 (2022)
- [40] Liu, Z., Lin, Y., Cao, Y., Hu, H., Wei, Y., Zhang, Z., Lin, S. & Guo, B. Swin transformer: Hierarchical vision transformer using shifted windows. *Proceedings Of The IEEE/CVF International Conference On Computer Vision*. pp. 10012-10022 (2021)
- [41] Loshchilov, I. Decoupled weight decay regularization. *ArXiv Preprint arXiv:1711.05101*. (2017)

- [42] Kool, W., Van Hoof, H. & Welling, M. Stochastic beams and where to find them: The gumbel-top-k trick for sampling sequences without replacement. *International Conference On Machine Learning*. pp. 3499-3508 (2019)
- [43] He, K., Zhang, X., Ren, S. & Sun, J. Deep residual learning for image recognition. *Proceedings Of The IEEE Conference On Computer Vision And Pattern Recognition*. pp. 770-778 (2016)